

Plasmonic Photocatalysis with Nonthermalized Hot Carriers

Shengxiang Wu, Yu Chen, and Shiwu Gao*

Beijing Computational Science Research Center, Beijing, 100193, China

(Received 5 April 2022; accepted 1 August 2022; published 17 August 2022)

Hot carriers generated by plasmonic damping have been suggested to promote photocatalysis, yet it remains unclear how the nonthermalized hot carriers dynamically activate and promote the energy transfer processes. Here, we present an Anderson-Newns model to describe the vibrational excitation and bond dissociation induced by plasmonic hot carriers. The nonthermal distribution of the hot carriers generated by plasmon damping is accounted for on equal footing with thermal carriers at a given temperature in the electron-molecule scattering. We found that the nonthermal electrons in the high energy region can, albeit in much smaller populations, provide an efficient and dominant channel for photodissociation especially in the low-temperature and quantum plasmon regime. Our model captures the wavelength dependence and reproduces the enhancement factors observed by experiments for oxygen dissociation on silver nanoparticles. It also paves a way to harvesting nonthermal plasmonic energy for photocatalysis in the quantum regime.

DOI: [10.1103/PhysRevLett.129.086801](https://doi.org/10.1103/PhysRevLett.129.086801)

Surface plasmons of metal nanoparticles (MNPs) have shown great potential for solar energy harvesting [1], photodetection [2,3], and photochemical energy conversion [4]. It was proposed [5–14] that hot electron-hole ($e-h$) pairs generated by plasmonic damping can open an electronic channel for photocatalysis that is otherwise inaccessible thermally. In bulk metals and large MNPs, these nonthermal carriers, which carry an initial energy equal to the plasmon quanta, can only survive for a very short lifetime (10–100 fs) due to the fast electron-electron and electron-phonon scatterings [15]. It remains unclear whether this hot-carrier mechanism may be inefficient in competition with a possible thermal heating mechanism [16,17]. However, as the size of the particle decreases, surface plasmons are expected to exhibit quantum behaviors in both their energies and lifetimes, leading to a significant increase in the lifetime with quantum oscillations in the small size limit [18–20]. It can be expected that surface plasmons in the quantum regime, and thus the associated hot carriers, may survive for much longer times than those in bulk metals and may be harvested for novel applications in nonthermal forms [21,22]. Indeed, a nonthermal distribution of plasmonic carriers has recently been identified in the injection and separation at the MNP-semiconductor interfaces using time-dependent density functional theory simulations [23,24]. Such a nonthermal process lasts for a few tens of femtoseconds through tunneling coupling, and finishes well ahead its relaxation within the MNPs.

Such an ultrafast and nonthermal injection offers new dimensions for electrochemistry and photochemistry, which shares a common tunneling coupling between the hot carriers and the chemisorbed molecules. In the

DIET (desorption induced by electronic transition) mechanism, photodissociation is initiated by an electron or a hole attachment from the MNP, forming a temporarily negative ion (TNI) resonance state. Subsequent evolution on the excited potential energy surface (PES) leads to vibrational excitation and bond dissociation [Fig. 1(a)] [5,25–30]. This DIET mechanism has been well established in the femtosecond laser desorption and dissociation by tunneling electrons [13,26,27,30]. It was recently adopted to analyze oxygen dissociation, invoking a single electron scattering event at the resonance energy [5,7,10]. However, the coupling to the full bath of nonthermal plasmonic hot carriers and its competition with possible thermal carriers have yet to be developed.

Here, we adopt the theory of hot carrier induced bond dissociation, based on the Anderson-Newns model coupled with a truncated harmonic oscillator, to calibrate and analyze the distribution of nonthermalized hot carriers of surface plasmons. The rates of vibrational excitation and dissociation induced by the plasmonic field are derived using the resonance electron-molecule scattering formalism, where the nonthermal carrier distribution is computed within the jellium model of electron spectra [31–33]. Independent of the material parameters, nonthermal electrons are found to provide an efficient channel, which outweighs the contribution from its thermal background, for vibrational excitation and bond dissociation especially at low temperatures and in the quantum limit. For oxygen dissociation on silver nanoparticles (NPs), our theory is able to capture the wavelength dependence of dissociation and reproduce the enhancement factors (EFs) of dissociation rate observed in experiments [6,13]. Our result reveals

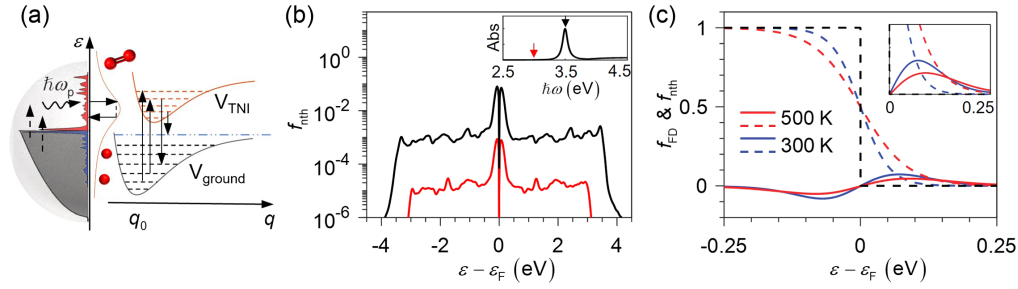


FIG. 1. Plasmon induced charge transfer from metal to molecule. (a) Schematic nonthermal carrier transfer and vibrational excitation induced by plasmonic damping. (b) Energy profile of the nonthermal carriers excited at resonance (black) and off-resonance (red). Nonthermal holes are represented in the opposite sign for illustration at the logarithmic scale. The inset displays the absorption spectrum. (c) Distribution of thermal (dashed line) and nonthermal (solid line) carriers at $T = 300$ K (blue) and $T = 500$ K (red). The inset highlights the intersections between thermal and nonthermal components. Parameters used in calculation: $D = 25$ nm, $\tau = 100$ fs.

the nonthermal carrier mechanism and unfolds the specific processes of surface plasmons. It also offers new avenues to the design of new plasmonic materials by optimizing carrier lifetime in the quantum plasmon regime.

The resonance electron-scattering formalism has been successful in the description of vibrational heating and reactions in femtosecond desorption [5,26–29], and molecular dissociation by tunneling electrons [30]. The model Hamiltonian of the metal-molecule system is recaptured as

$$\begin{aligned}
 H &= H_p + H_e + H_i \\
 &= \frac{p^2}{2m} + V(q) + \sum_k \varepsilon_k c_k^\dagger c_k + \varepsilon_a c_a^\dagger c_a \\
 &\quad + \sum_k (\nu_{ak} c_a^\dagger c_k + \text{H.c.}) - \xi q,
 \end{aligned} \quad (1)$$

where H_p , H_e , and H_i are the Hamiltonians of the molecular vibration, the electron subsystem, and the electron-vibration coupling. For simplicity, the vibration of the molecule is treated as a truncated harmonic oscillator with reaction coordinate q and vibrational energy $\hbar\Omega$. The $\{\varepsilon_k, |k\rangle\}$ are the electron spectra, which are calculated from the jellium model of spherical MNPs (see Supplemental Material) [34]. The local molecular state $|a\rangle$, after hybridization with MNPs, forms a negative ion resonance with local density of states, $\rho_a = (1/\pi)[\Delta_a/(\varepsilon - \varepsilon_a)^2 + \Delta_a^2]$. Here, $\Delta_a = \sum_k \pi \nu_{ak}^2 \delta(\varepsilon - \varepsilon_k)$ effectively accounts for the tunneling coupling between the metal electrons and the molecule. The linear coupling $\xi = -\lambda c_a^\dagger c_a$ describes the force acting on the molecule upon excitation, and $\lambda = \sqrt{(\hbar/2m\Omega)(d/dq)V_{\text{TNI}}|_{q=q_0}}$ is the electron-vibrational coupling constant.

Following the theory of vibrational heating [27–29], the vibrational transition rate $W_{n \rightarrow n'}$ from state n to state n' of the molecular vibration is described as

$$\begin{aligned}
 W_{n \rightarrow n'} &= \frac{4\Delta_a^2}{\pi\hbar} \int d\varepsilon f(\varepsilon)[1 - f(\varepsilon + \delta\varepsilon)] \\
 &\quad \times \left| \sum_m \frac{\langle n'|m\rangle \langle m|n\rangle}{\varepsilon - n\hbar\Omega - \varepsilon_a - m\hbar\Omega + i\Delta_a} \right|^2, \quad (2)
 \end{aligned}$$

where $f(\varepsilon)$ is the energy distribution of the electron gas, which is now expanded to include both thermal and nonthermal distribution components as detailed below, and $\delta\varepsilon = (n - n')\hbar\Omega$ is the energy transfer between the electronic bath and the molecule. The Franck-Condon factors between ground and excited states $\langle n'|m\rangle$ (and $\langle m|n\rangle$) are evaluated analytically [37], wherein the PESs of the ground state $|n\rangle$ and TNI state $|m\rangle$ are modeled as (truncated) harmonic oscillators (see Supplemental Material [34]). The electron-vibrational coupling constant is chosen such that the $W_{1 \rightarrow 0}$ rate reproduces the experimental vibrational damping rate due to the excitation of electron-hole pairs in metals [38,39].

To model the plasmonic hot carriers in a steady state experiment generated by CW lasers, the distribution function f is now expanded to include both the thermal distribution f_{FD} (the Fermi-Dirac distribution) at a given temperature and a novel term for nonthermalized hot carriers f_{nth} , which are generated by Landau damping of surface plasmons.

$$f = \begin{cases} f_{\text{FD}}(\varepsilon, T), & \text{light off,} \\ f_{\text{FD}}(\varepsilon, T) + f_{\text{nth}}, & \text{light on,} \end{cases} \quad (3a)$$

$$f_{\text{nth}} = \frac{\delta\rho(\varepsilon, T, \hbar\omega)}{\rho_{\text{DOS}}(\varepsilon)}, \quad (3b)$$

where ρ_{DOS} is the electronic density of states and $\delta\rho$ is the nonthermal carrier distribution derived from Landau damping of surface plasmon as documented in earlier literature (see Supplemental Material) [31,33,34].

Figure 1(b) shows the nonthermal carrier distributions of a $D = 25$ nm NP excited by two laser frequencies at

resonance (3.5 eV, black) and off resonance (3 eV, red), respectively, while the inset shows the absorption spectrum. Three prominent features can be observed. First, there is a strong resonance enhancement, by more than 2 orders of magnitude, in both absorption and nonthermal carrier production at the plasmon resonances. Second, at a given photon energy $\hbar\omega$, the distributions of nonthermal carriers are within the range from ε_F to $\varepsilon_F + \hbar\omega$ for electrons and from $\varepsilon_F - \hbar\omega$ to ε_F for holes, which is as expected by energy conservation in Landau damping. Third, most of the nonthermal carriers are distributed in the vicinity of the Fermi level, especially at shorter electron lifetimes. This is because the nonthermal carrier distributions are partly determined by the populations of the thermal e - h pairs during Landau damping. As the lifetime τ increases, the distribution becomes more nonthermal and an appreciable fraction of distribution shows up in both the high-energy electron and hole regions (see Supplemental Material [34]).

Figure 1(c) compares the nonthermal distribution with the thermal ones at two different temperatures, 300 and 500 K. Obviously the thermal carriers are mainly distributed within the energy range $[-k_B T, k_B T]$ and decay exponentially away from the Fermi level [dashed lines in Fig. 1(c)]. Despite the fast relaxation and small population, the nonthermal carriers (the solid curves) always outweigh the thermal carriers at high energies. Indeed, as shown in the inset of Fig. 1(c), at each temperature the nonthermal distribution always intersects with the thermal one at a crossing energy point, beyond which the nonthermalized distribution f_{nth} starts to dominate. With the thermal and nonthermal carrier distributions defined and calibrated, one can now analyze how the nonthermal carriers participate in electron-vibrational coupling and chemical bond dissociation in a thermal background.

As an application of the above formulation, we analyze first the vibrational excitation and dissociation of O_2 on Ag NPs, where a large group of experiments in plasmon-mediated photocatalysis has been reported. Model parameters are extracted from the chemisorbed O_2 on Ag(100) with $\Delta_a = 0.6$ eV, $\varepsilon_a = 2.4$ eV, which corresponds to the O_2 $2\pi^*$ resonance, and $\hbar\Omega = 0.10$ eV is the vibrational energy of the stretch mode [7]. The dissociation barrier $D_0 = 1.17$ eV accommodates 11 bound states, and thus the $n = 12$ state is treated as the dissociation state in the truncated harmonic oscillator approximation.

Figure 2 analyzes the rate of vibrational excitation contributed from different parts of the thermal and nonthermal distributions. In Fig. 2(a), the energy spectrum of carriers are divided into three regions: regions I, III primarily contain the plasmon-induced nonthermal holes and electrons, respectively. While region II within $(-0.25$ eV, 0.25 eV) contains both the thermal $f_{FD}(\varepsilon, T)$ and nonthermal f_{nth} components near the Fermi level, but is obviously dominated by thermal carriers around the Fermi level.

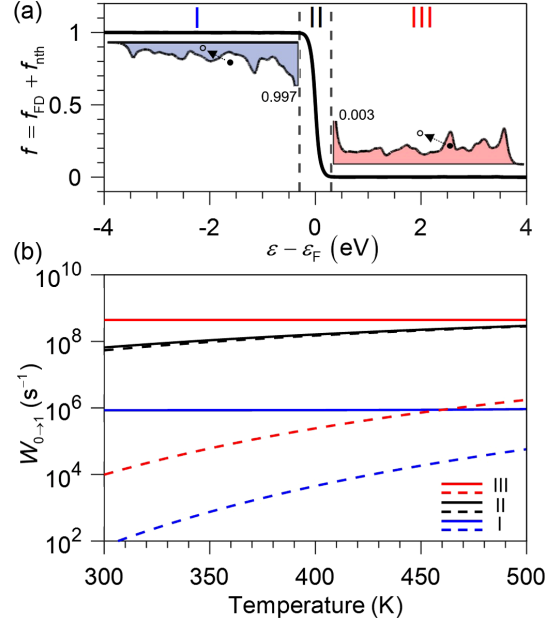


FIG. 2. The vibrational excitation is primarily driven by high-energy nonthermal carriers. (a) Total distribution of carriers in $D = 25$ nm silver nanosphere at $T = 400$ K. Carriers are segmented into three regions, the thermal excitation around the Fermi level is mostly embedded in region II, while regions I and III contain primarily nonthermal holes and electrons, respectively. The arrow schematically shows the inelastic scattering of the electron from an occupied state to an unoccupied state. (b) Temperature-dependent vibrational excitation, $W_{0 \rightarrow 1}$, evaluated in dark (dashed line) and resonant (solid line) light illumination. In all calculations, an electron lifetime of $\tau = 100$ fs is used.

Figure 2(b) shows the rate of vibrational excitation $W_{0 \rightarrow 1}$ as a function of temperature induced by hot carriers from the three regions, respectively. The black solid line is the excitation rate from carriers in region II, which is almost the same as the case without illumination (black dashed line). This is because the carriers near the Fermi level are dominated by the thermalized ones, as shown in Fig. 2(a). However, the nonthermal carriers drastically increase the vibrational excitation in both region I (blue lines) and region III (red lines) when the light is turned on. They are also temperature independent due to their nonthermal character. Overall, the nonthermal electrons in region III dominate the total transition rates by more than 2 orders of magnitude because the high-energy nonthermal electrons are energetically more favorable in the vibrational coupling with the unoccupied $2\pi^*$ orbital. This trend is even more drastic for the transition from the ground state to higher vibrational states and the dissociation state $W_{0 \rightarrow 12}$ (see Supplemental Material [34]) where it requires a much larger nonadiabatic energy transfer and the direct thermal dissociation becomes thus even less efficient. It is worth mentioning that although phonon induced vibrational transition is inefficient in the adsorbed molecules, thermal distribution of the vibrational states $p_n(T)$ for $n > 1$, which

is in equilibrium with the phonon bath of the MNPs via anharmonic coupling, is implicitly included in our modeling, and should account for the dominant part of the purely thermal effect.

Next, we discuss the rate of dissociation of O_2 and CO on silver nanoparticles under light illumination at resonance plasmon excitation. Vibrational transitions from all thermally populated bound states in the potential well are included in the rate of dissociation, $R_{\text{dis}} = \sum_n p_n W_{n \rightarrow 12}$ where p_n is the thermal population of vibrational state n at temperature T . This rate includes both the thermal and nonthermal carrier populations. We neglected phonon induced vibrational transitions because the phonon bands of silver are within 30 meV [40], which is much smaller than the vibrational energy $\hbar\Omega$ of the adsorbed molecules. Vibrational excitation by phonon scatterings would require multiphonons (>3) processes and is expected to be inefficient.

Figure 3 shows the dissociation rates for O_2 (black) and CO (red) on silver NPs with (solid line) and without (dashed line) light illumination. The nonthermal distribution f_{nth} was calculated assuming electron lifetime $\tau = 100$ fs. At low temperatures, the reaction rates with illumination (solid line) are enhanced by several orders of magnitude compared with the dark condition (dashed line) for both O_2 and CO, as thermal populations of vibrational states are small, and the dissociation rate is dominated by the activation from the low-lying bound states $n = 0$ and $n = 1$ at low T . Therefore, R_{dis} is significantly enhanced because the energy-demanding transitions $W_{0 \rightarrow 12}$ and $W_{1 \rightarrow 12}$ are only accessible by the energetic nonthermal electrons (see Supplemental Material [34]). As the temperature increases, the higher vibrational modes are also partially populated, thus the required energy to dissociate the molecules is effectively reduced. This is similarly

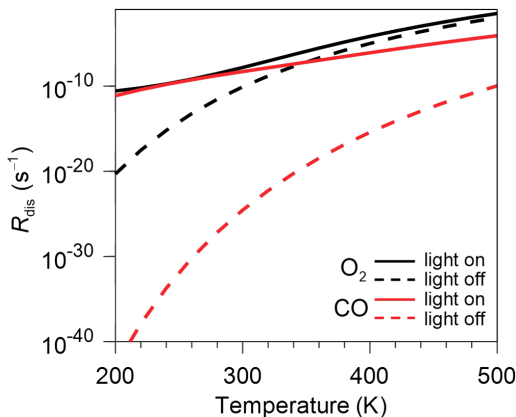


FIG. 3. Reaction rates without (dashed lines) and with (solid lines) resonant light illumination at $\hbar\omega = 3.5$ eV of O_2 (black) and CO (red). The adsorbate-specific parameters are adopted from Ref. [7] for O_2 and Refs. [5,41,42] for CO. In all calculations, $\tau = 100$ fs is used.

shown as in Fig. 2(b), where the difference between with and without illumination is moderate in region II and the contributions from regions I and III start to approach the thermal excitations at high temperatures. The effect of nonthermal carriers is more drastic for molecules with larger dissociation barriers, say 5 eV, which reasonably represents for CO on metal surfaces [41,42]. Because of the higher dissociation barrier, the dissociation rates are generally several orders of magnitude smaller, and is completely dominated by the nonthermal carriers even at high temperatures. A more detailed analysis of the dissociation rate with contribution from different vibrational states is given in the Supplemental Material [34].

We have also calculated the wavelength-dependent reaction rates by varying the photon energies [see Fig. 4(a) and Supplemental Material [34]]. In both cases, they follow qualitatively the absorption spectra with a strong enhancement at the plasmon resonance as found in experiments. They also show additional minor shoulder on the left (O_2) or the right (CO) side of the plasmon resonances. This shoulder comes from the electronic resonance effect

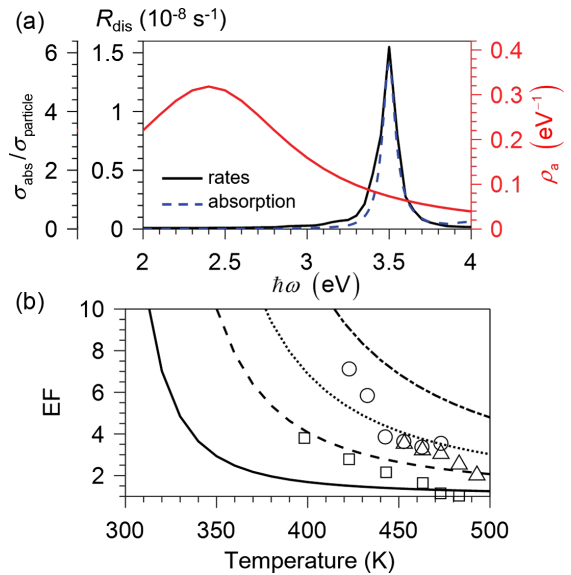


FIG. 4. (a) Wavelength-dependent reaction rates of O_2 . The reaction rates largely follow the plasmon resonance (absorption). The minor peaks on the left could be an independent signature that distinguish hot carrier effect from thermal heating. The red line (ρ_a) represents the local density of states for the negative ion O_2^- resonance. $\tau = 100$ fs is used in calculation. (b) Enhancement factor of plasmon-mediated O_2 dissociation on Ag NPs. Enhancement factor (EF) is defined as the ratio between reaction rates with and without illumination. The nonthermal carriers are evaluated at various electron relaxation time $\tau = 10, 50, 100, 200$ fs (solid to dash-dotted line). The EF of three reactions with O_2 dissociation being the rate-limiting step, (circle) ethylene epoxidation, (triangle) NH_3 oxidation, and (square) CO oxidation are digitized from experimental data in Ref. [6]. The nonthermal carriers are all evaluated at resonance condition $\hbar\omega = 3.5$ eV.

contained in the electron propagator [Eq. (2)]. The minor peak arises simply because the plasmon-resonance offsets from the TNI resonance and may be another signature for the nonthermal reaction mechanism.

As another comparison with experiments, Fig. 4(b) shows the enhancement factors (EF), which are derived from the ratio between the solid and dashed lines in Fig. 3. The experimental data are digitized from Ref. [6] for ethylene epoxidation, NH_3 oxidation, and CO oxidation, where the dissociation of O—O bond is commonly the rate-limiting step. The calculated EF lies in the reasonable range of the experimental data using a relaxation time $\tau = 10\text{--}200$ fs, which is typical for silver reported in ultrafast studies [15]. Given the sensitive energy dependences and temperature dependences of the electronic lifetime τ in MNPs, it is thus inappropriate to make direct comparison between the experimental EFs, which are diverse themselves, with any EF curves at a fixed τ value. Nevertheless, we can mention that with a simple temperature-dependent lifetime $\tau \propto 1/T^2$, as expected from the Fermi liquid theory (see Fig. S8 in Supplemental Material [34,43]), it is possible to achieve a better fitting between the model and the experimental data. This should, however, be viewed with caution because the lifetime parameter depends on many competing factors such as surface scattering, adsorbates, and adsorption sites, whose temperature dependences are much more complex than the bulk electron gas, and whose discussion is beyond the scope of the present model. In general, the EF increases with τ since more nonthermal carriers are populated at higher energy state at longer τ . Therefore, it may serve as a guiding principle for the design of plasmonic photocatalysis with longer electronic lifetime in order to optimize the plasmonic catalytic performance. A promising route to this end is to employ MNPs-semiconductor hybrids, in which fast injection and spatial separation of hot carriers can significantly increase the effective lifetime of the hot carriers [22] and can thus improve the efficiency of plasmonic photocatalysis. Alternatively, one can use smaller MNPs, whose plasmon lifetime can be increased due to the suppression of decay channels, but this consideration should be weighed against potential tradeoffs in the reduced absorption cross sections and the unwished frequency shift of plasmon resonances.

In conclusion, we developed a quantum-mechanical model for vibrational excitation and molecular dissociation mediated by nonthermal carriers and applied it in molecular dissociation on silver nanoparticles. Our analysis of O_2 dissociation captures the wavelength dependences of dissociation rates and reproduces the enhancement factors induced by the surface plasmons. Our findings reveal the nonthermal mechanism and the underlying dynamics involved in resonance electron-vibrational coupling and plasmonic hot carrier enhancement. It also paves a

promising way for plasmonic photocatalysis and other energy conversion application using surface plasmons.

This work was supported by the National Natural Science Foundation of China (11934003, 21961132023, U1930402), and the National Key R&D Program of MOST of China (2017YFA0303404). The authors would like to thank Dr. Yang Jiao for fruitful discussions.

*swgao@csrc.ac.cn

- [1] U. Aslam, S. Chavez, and S. Linic, Controlling energy flow in multimetallic nanostructures for plasmonic catalysis, *Nat. Nanotechnol.* **12**, 1000 (2017).
- [2] F. Neubrech, A. Pucci, T.W. Cornelius, S. Karim, A. García-Etxarri, and J. Aizpurua, Resonant Plasmonic and Vibrational Coupling in a Tailored Nanoantenna for Infrared Detection, *Phys. Rev. Lett.* **101**, 157403 (2008).
- [3] M. W. Knight, H. Sobhani, P. Nordlander, and N. J. Halas, Photodetection with active optical antennas, *Science* **332**, 702 (2011).
- [4] U. Aslam, V.G. Rao, S. Chavez, and S. Linic, Catalytic conversion of solar to chemical energy on plasmonic metal nanostructures, *Nature Catalysis* **1**, 656 (2018).
- [5] T. Olsen, J. Gavnholt, and J. Schiøtz, Hot-electron-mediated desorption rates calculated from excited-state potential energy surfaces, *Phys. Rev. B* **79**, 035403 (2009).
- [6] P. Christopher, H. Xin, and S. Linic, Visible-light-enhanced catalytic oxidation reactions on plasmonic silver nanostructures, *Nat. Chem.* **3**, 467 (2011).
- [7] P. Christopher, H. Xin, A. Marimuthu, and S. Linic, Singular characteristics and unique chemical bond activation mechanisms of photocatalytic reactions on plasmonic nanostructures, *Nat. Mater.* **11**, 1044 (2012).
- [8] S. Mukherjee, F. Libisch, N. Large, O. Neumann, L. V. Brown, J. Cheng, J. B. Lassiter, E. A. Carter, P. Nordlander, and N. J. Halas, Hot electrons do the impossible: Plasmon-induced dissociation of H_2 on Au, *Nano Lett.* **13**, 240 (2013).
- [9] S. Mukherjee, L. Zhou, A. M. Goodman, N. Large, C. Ayala-Orozco, Y. Zhang, P. Nordlander, and N. J. Halas, Hot-electron-induced dissociation of H_2 on gold nanoparticles supported on SiO_2 , *J. Am. Chem. Soc.* **136**, 64 (2014).
- [10] C. Boerigter, U. Aslam, and S. Linic, Mechanism of charge transfer from plasmonic nanostructures to chemically attached materials, *ACS Nano* **10**, 6108 (2016).
- [11] C. Boerigter, R. Campana, M. Morabito, and S. Linic, Evidence and implications of direct charge excitation as the dominant mechanism in plasmon-mediated photocatalysis, *Nat. Commun.* **7**, 10545 (2016).
- [12] L. Zhou, D. F. Swearer, C. Zhang, H. Robotjazi, H. Zhao, L. Henderson, L. Dong, P. Christopher, E. A. Carter, P. Nordlander, and N. J. Halas, Quantifying hot carrier and thermal contributions in plasmonic photocatalysis, *Science* **362**, 69 (2018).
- [13] E. Kazuma, M. Lee, J. Jung, M. Trenary, and Y. Kim, Single-molecule study of a plasmon-induced reaction for a

- strongly chemisorbed molecule, *Angew. Chem. Int. Ed.* **59**, 7960 (2020).
- [14] D. Devasia, A. Das, V. Mohan, and P. K. Jain, Control of chemical reaction pathways by light-matter coupling, *Annu. Rev. Phys. Chem.* **72**, 423 (2021).
- [15] F. Evers, C. Rakete, K. Watanabe, D. Menzel, and H.-J. Freund, Two-photon photoemission from silver nanoparticles on thin alumina films: Role of plasmon excitation, *Surf. Sci.* **593**, 43 (2005).
- [16] Y. Dubi and Y. Sivan, “Hot” electrons in metallic nanostructures-non-thermal carriers or heating?, *Light* **8**, 89 (2019).
- [17] Y. Dubi, I. W. Un, and Y. Sivan, Thermal effects: An alternative mechanism for plasmon-assisted photocatalysis, *Chem. Sci.* **11**, 5017 (2020).
- [18] U. Kreibig, Electronic properties of small silver particles: The optical constants and their temperature dependence, *J. Phys. F* **4**, 999 (1974).
- [19] U. Kreibig and L. Genzel, Optical absorption of small metallic particles, *Surf. Sci.* **156**, 678 (1985).
- [20] Z. Yuan and S. Gao, Landau damping and lifetime oscillation of surface plasmons in metallic thin films studied in a jellium slab model, *Surf. Sci.* **602**, 460 (2008).
- [21] S. K. Cushing, C.-J. Chen, C. L. Dong, X.-T. Kong, A. O. Govorov, R.-S. Liu, and N. Wu, Tunable nonthermal distribution of hot electrons in a semiconductor injected from a plasmonic gold nanostructure, *ACS Nano* **12**, 7117 (2018).
- [22] G. Tagliabue, J. S. DuChene, M. Abdellah, A. Habib, D. J. Gosztola, Y. Hattori, W.-H. Cheng, K. Zheng, S. E. Canton, R. Sundararaman, J. Sá, and H. A. Atwater, Ultrafast hot-hole injection modifies hot-electron dynamics in Au/*p*-GaN heterostructures, *Nat. Mater.* **19**, 1312 (2020).
- [23] J. Ma and S. Gao, Plasmon-induced electron-hole separation at the Ag/TiO₂(110) interface, *ACS Nano* **13**, 13658 (2019).
- [24] J. Ma, X. Zhang, and S. Gao, Tunable electron and hole injection channels at plasmonic Al-TiO₂ interfaces, *Nanoscale* **13**, 14073 (2021).
- [25] N. S. Wingreen, K. W. Jacobsen, and J. W. Wilkins, Inelastic scattering in resonant tunneling, *Phys. Rev. B* **40**, 11834 (1989).
- [26] J. W. Gadzuk, Inelastic resonance scattering, tunneling, and desorption, *Phys. Rev. B* **44**, 13466 (1991).
- [27] S. Gao, D. G. Busch, and W. Ho, Femtosecond dynamics of electron-vibrational heating and desorption, *Surf. Sci.* **344**, L1252 (1995).
- [28] S. Gao, B. I. Lundqvist, and W. Ho, Hot-electron-induced vibrational heating at surface: Importance of a quantum-mechanical description, *Surf. Sci.* **341**, L1031 (1995).
- [29] S. Gao, Quantum kinetic theory of vibrational heating and bond breaking by hot electrons, *Phys. Rev. B* **55**, 1876 (1997).
- [30] B. C. Stipe, M. A. Rezaei, W. Ho, S. Gao, M. Persson, and B. I. Lundqvist, Single-Molecule Dissociation by Tunneling Electrons, *Phys. Rev. Lett.* **78**, 4410 (1997).
- [31] A. Manjavacas, J. G. Liu, V. Kulkarni, and P. Nordlander, Plasmon-induced hot carriers in metallic nanoparticles, *ACS Nano* **8**, 7630 (2014).
- [32] A. O. Govorov and H. Zhang, Kinetic density functional theory for plasmonic nanostructures: Breaking of the plasmon peak in the quantum regime and generation of hot electrons, *J. Phys. Chem. C* **119**, 6181 (2015).
- [33] J. G. Liu, H. Zhang, S. Link, and P. Nordlander, Relaxation of plasmon-induced hot carriers, *ACS Photonics* **5**, 2584 (2018).
- [34] See Supplemental Material at <http://link.aps.org/supplemental/10.1103/PhysRevLett.129.086801> for electronic structure calculation, plasmon-induced generation of nonthermal hot carriers, Franck-Condon factors evaluation, additional wavelength-dependent study of photocatalysis, and the description of improved correlation with experiments using temperature-dependent relaxation time, which includes Refs. [35,36].
- [35] P. B. Johnson and R. W. Christy, Optical constants of the noble metals, *Phys. Rev. B* **6**, 4370 (1972).
- [36] A. O. Govorov, H. Zhang, and Y. K. Gun’ko, Theory of photoinjection of hot plasmonic carriers from metal nanostructures into semiconductors and surface molecules, *J. Phys. Chem. C* **117**, 16616 (2013).
- [37] F. Iachello and M. Ibrahim, Analytic and algebraic evaluation of Franck-Condon overlap integrals, *J. Phys. Chem. A* **102**, 9427 (1998).
- [38] B. N. J. Persson and M. Persson, Vibrational lifetime for Co adsorbed on Cu(100), *Solid State Commun.* **36**, 175 (1980).
- [39] I. Lončarić, M. Alducin, J. I. Juaristi, and D. Novko, Co stretch vibration lives long on Au(111), *J. Phys. Chem. Lett.* **10**, 1043 (2019).
- [40] J. W. Arblaster, Thermodynamic properties of silver, *J. Phase Equilib. Diffus.* **36**, 573 (2015).
- [41] B. W. J. Chen, D. Kirvassilis, Y. Bai, and M. Mavrikakis, Atomic and molecular adsorption on Ag(111), *J. Phys. Chem. C* **123**, 7551 (2019).
- [42] S. Amaya-Roncancio, L. Reinaudi, and M. C. Gimenez, Adsorption and dissociation of Co on metal clusters, *Mater. Today Commun.* **24**, 101158 (2020).
- [43] P. Coleman, *Introduction to Many-Body Physics* (Cambridge University Press, Cambridge, 2015).